Evaporation of single droplets of multicomponent liquid fuel blends at elevated temperatures

W. Dang[1*], W. Zhao[2], S. K. Menon[3]

[1]Graduate Research Assistant, Mechanical & Industrial Engineering, Louisiana State University, United States

[2]Undergraduate Researcher, Mechanical & Industrial Engineering, Louisiana State University, United States

[3]Assistant Professor, Mechanical & Industrial Engineering, Louisiana State University, United States

Abstract

The atomization and evaporation of fuels plays an indispensable role in the combustion process of direct injection engines. There is considerable interest in understanding the physics of the evaporation process of multi-component fuels, particularly at elevated temperature and pressure conditions representative of internal combustion (IC) engines. In this work, the evaporation process of multi-component fuels is investigated by considering different mixture ratios of *iso*-octane and *n*-heptane at atmospheric pressure but elevated temperature conditions. Single droplet trains of different fuel blends are generated in a constant volume chamber whose temperature and pressure can be controlled as desired. The evaporation process of the droplets is visualized using a camera, which allows the change in droplet size to be measured as a function of time. The evaporation of single droplets of pure fuels is also calculated using a numerical model. The evaporation behavior is studied as a function of different ambient temperatures and fuel mixtures. Good agreement is observed between the model predictions and experimental measurements for the pure fuels. The evaporation rate of n-heptane is observed to be higher than that of *iso*-octane as expected. Increase in ambient temperature is seen to increase the evaporation rate of fuel droplets. Increasing the concentration of n-heptane in the fuel mixture is seen to initially increase the evaporation rate. However, the highest evaporation rate is observed for an intermediate fuel blend and not for the case of pure n-heptane.

Keywords: Droplet evaporation; Multicomponent fuels

Introduction

The use of fuel sprays is ubiquitous in power generation applications utilizing liquid hydrocarbon fuels. The spray provides a pathway to introduce fuel into the power generation device such as a reciprocating-type internal combustion (IC) engine or a gas turbine engine. Beyond simply introducing fuels into the device, the fuel injection system plays a critical role in the subsequent spray breakup, atomization, evaporation, and mixing of fuel with air. While fundamental investigations into each of these processes have been extensively carried out, several recent advances in IC engines motivate us to revisit aspects of liquid fuel evaporation which forms a key component of the fuel-air mixing process.

One of the advances relates to advanced combustion cycles. Engine researchers are seeking to tackle fuel efficiency and emission reduction issues simultaneously by increasingly targeting a form of combustion which is a superposition of conventional gasoline and diesel cycles. Several strategies that blend the high compression ratio of diesel engines with premixing inherent in gasoline engines have been extensively researched. Two examples of such strategies are the low temperature gasoline compression (LTGC) engines [1] and reactivity controlled compression ignition (RCCI) engines [2]. For these advanced engine cycles, the environment into which fuel is injected is considerably different from that in a conventional IC engine. The ambient conditions for the spray has features such as high temperature, high pressure, and partially reacted fuel components. Figure 1 shows the landscape of advanced combustion strategies aimed at achieving low temperature combustion with gasoline and diesel fuels [3]. The ambient conditions strongly affect fuel spray and atomization processes. Ambient temperature and pressure critically control the droplet size, speed, and penetration. Ambient temperature and chemical composition affect the evaporation rate and fuel-air mixing.

Another key aspect affecting the fuel-air mixing process is the fuel itself and its physical properties. This is particularly true for novel and emerging bio-fuels that could be drop-in replacements or blended with conventional fossil fuels [4]. Ethanol is commonly blended with gasoline in varying amounts aiding in the reduction of greenhouse gas emissions such as CO_2, and reducing fossil fuel costs. Even gasoline and diesel are essentially mixtures of many components, thus making the understanding of multi-component fuel mixtures all the more relevant. Finally, engine downsizing is a trend that has dominated the IC engine market especially in the passenger car

sector. The key idea is that IC engines can be operated more efficiently by reducing the engine size and boosting the power by turbocharging the intake air for transient conditions that require excess power [5]. Downsizing with turbo-boosting impacts fuel evaporation in several ways including: increased ambient pressures, increased surface-to-volume ratio affecting heat transfer processes, and fuel wetting causing liquid fuel to impact the cylinder walls.

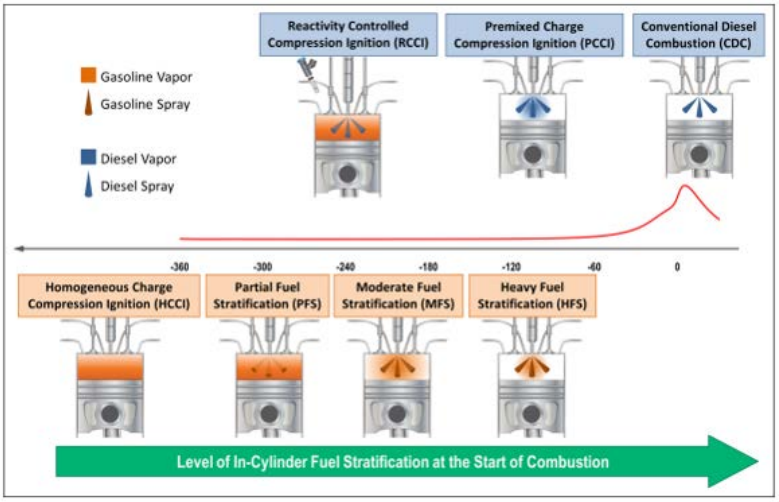

Figure 1: Advanced combustion cycles for IC engines [3].

The issues mentioned above relating to advances in IC engines provide motivation to study fuel spray, evaporation, and mixing processes at ambient conditions of high temperature, high pressure, and partially reacted components, using emerging bio-fuels and multi-component fuels. The current work presents a first step in that direction where we seek to investigate the effect of ambient temperature and fuel blends on the evaporation rate of single droplets. While this configuration is considerably different from the dense spray and turbulent flow environment in an actual engine chamber, it isolates and provides fundamental understanding of the droplet evaporation process. The approach of isolating single droplets and studying their evaporation in convective flow has been pursued extensively by previous researchers using experimental and computational approaches. Review papers by Sazhin [6], Birouk [7], Peng [8], and Sirignano [9], comprehensively cover various experimental and computational efforts. Key differences that set apart the present work is the initial size of the droplets (50 μ.m) which is smaller than what investigations have focused on in the past (>100 μ.m) and the fuel composition. In this work, we seek to identify the sensitivity of the droplet evaporation rate to the blending ratio of primary reference fuels (PRF), *iso*-octane and *n*-heptane. The interest in PRF fuel blends arises from the standard use of such fuels for measuring auto-ignition quality through research octane and motor octane numbers (RON and MON). Under certain conditions, the ignition and combustion processes of PRF's can simulate similar processes occurring with practical fuels, which are blends of many different components [10]. This motivates the study of evaporation characteristics of PRF fuels and their blends.

Following the motivations described above, an experimental approach is pursued to study the evaporation process of single liquid fuel droplets in a heated environment under convective flow conditions. As mentioned previously, this study serves as a first step towards the overall goal of understanding fuel evaporation and mixing at conditions relevant to advanced IC engines. The experimental setup is described next wherein monodisperse fuel droplets generated by a piezo-electric droplet generator are injected into a heated ambient environment with an initial velocity. The test conditions of initial droplet size, droplet velocity, ambient temperature, and fuel blends, which are investigated in this work are described next. A computational model based on classical droplet evaporation theory is described along with model assumptions. Results are presented for the various test cases comparing experimental measurements with model predictions. Following a discussion of the results, conclusions and future research directs are presented.

Experimental Methods

Experimental setup

The experiment setup is shown in Figure 2. A piezoelectric droplet generator made by MicroFab Inc., which can produce single droplet trails of controlled size and frequency, is placed inside a pressure chamber with air as the carrier gas. When an external pulse generated by Microfab JetDrive V (CT-M5-01) is applied, the piezoelectric actuator expands or contracts according to the polarity of the waveform. This fast deformation results in droplet

formation at nozzle tip if an equilibrium condition is maintained at the meniscus of the 30µm nozzle orifice. A pressure controller is used to provide stable backpressure to adjust the force balance at the meniscus. The controller is connected to a vacuum pump as well as a compressed air source allowing it to maintain positive or negative backpressure. The droplet size and initial velocity can be controlled using the amplitude and shape of the voltage waveform pulse applied to the piezoelectric actuator. The frequency of the pulse controls the droplet spacing. A machine vision camera (Sentech STC-MB33USB) mounted on a vertical traverse is used to obtain real-time images of the droplets at different locations after being injected from the nozzle. The camera has optical access into the chamber through the quartz windows located on either side of the pressure chamber. An LED strobe located at the opposite end of the chamber provides the light source for the camera. A closed-loop temperature control system consisting of a PID controller heating wire is used to control the temperature of the chamber. In this work, all the measurements are carried out at atmospheric pressure. However, it is worth noting that we have previously demonstrated operation of the droplet generator at higher than ambient pressures. As mentioned in the introduction, experiments were carried out for various blends of PRF's. The fuel mixtures were prepared by transferring *iso*-octane and *n*-heptane into scaled glass vials with pipettes. The blending ratio here is based on volumetric mixing ratio of the two reference fuels.

To conduct the tests, the chamber doors are closed and the chamber is pressurized to the desired ambient pressure. In this case, all tests were conducted at atmospheric conditions. Next, the temperature controller is set to the desired set-point. Once the desired temperature is reached inside the chamber, the pressure controller is used to first purge some of the fuel thereby producing a well-defined liquid meniscus visualized on a live video stream from the camera. Next, using the pressure controller, the meniscus is carefully aligned with the exit plane of the glass nozzle. Once aligned, the desired waveform pulse is applied to produce the liquid droplet train with the required frequency. The camera is used to take images of the droplets at various downstream locations from the nozzle by moving it using the vertical traverse.

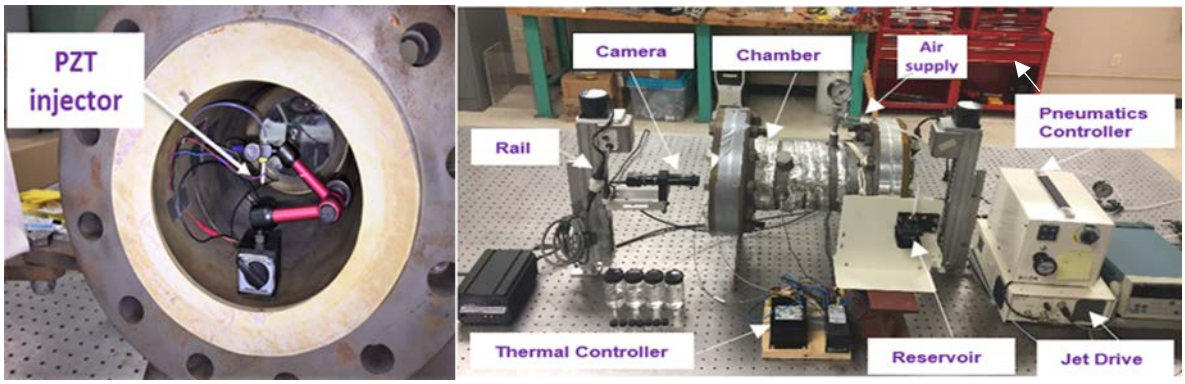

Figure 2: Experimental setup and piezoelectric injector

Diagnostics and Data Processing

The droplet dispensing process is captured by the camera as described above. The LED strobe light located on the opposite end of the chamber across from the camera is pulsed at the same frequency as that of the droplet generator. This results in a static trail of droplets located at different distances downstream from the nozzle exit plane. The droplet trail is recorded by the camera by moving it on the vertical traverse. After a series of images are captured by the camera, a post-processing software, Image J [11], was used to locate and size the droplets in each image. The same software was also used to measure the vertical distance between the droplets. One of the major advantages of this technique is its high efficiency and uniformity allowing for a large number of images to be processed using techniques such as FFT and background subtraction, with a single script.

Test Conditions

Tests were carried out for various blends of the PRF's at two different ambient temperature conditions of 40°C and 50°C. All tests were carried out at atmospheric pressure conditions. Depending on the case, different voltage profiles had to be applied in order to achieve a stable droplet generation. The voltage waveform has a shape as shown in Figure 3. Table 1 shows the test conditions for cases studied in this work. For

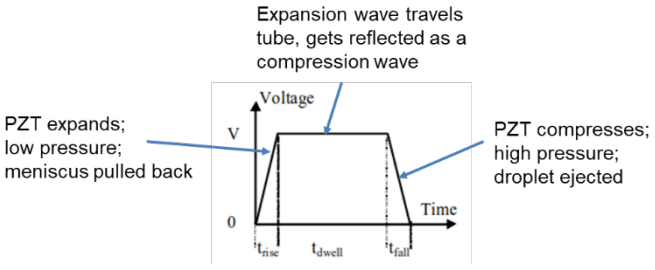

Figure 3: Voltage waveform applied for droplet generation.

all test cases, the signal frequency had a constant value of 700Hz and rise/fall time was set to be 5µs. Table 1 also shows the initial velocity and initial diameter of the droplet as observed for each test case.

Test #	1	2	3	4	5	6	7	8	9	10	11	12
PRF Ratio (*iso*-octane: *n*-heptane)	100:0	0:100	20:80	40:60	60:40	80:20	100:0	0:100	20:80	40:60	60:40	80:20
Temperature (ºC)	40	40	40	40	40	40	50	50	50	50	50	50
Voltage (V)	25	24	24	23	30	24	17	20	25	16	25	22
Dwell time (µs)	55	60	55	42	55	54	50	40	59	48	63	55
Initial velocity (m/s)	0.81	0.63	0.39	1.14	0.71	0.58	0.56	0.58	0.52	0.81	0.72	0.41
Initial diameter (µm)	68.7	62.7	58.4	60.6	70.6	67.5	54.3	67.2	59.2	56.7	56.2	64

Table 1. Test Conditions and input parameters

Computational Methods

Droplet vaporization model

The Abramzon and Sirignano model [11] which builds upon the classical droplet evaporation model is used in this work to simulate the evaporation of a single liquid fuel droplet. The model considers the evaporation of a moving fuel droplet while accounting for the convective heat and mass transport by employing a film thickness around the droplet. The film consists of a mixture of evaporated fuel and ambient gas. Since the model is extensively described in literature [6], [11], only a brief overview of the model is provided here. The model makes several assumptions as below:

- A quasi-steady approximation is made for the gas phase heat and mass transfer.
- The droplet has a single downward velocity component while the ambient gas is stationary.
- Thermo-physical properties are evaluated at some reference conditions and assumed to be constant.
- The distribution of temperature and fuel vapor concentration along the droplet surface is assumed to be uniform.
- An 'infinite conductivity model' is assumed which assumes a spatially uniform but time-varying temperature within the droplet.
- The velocity field within the moving droplet is disregarded.

The model solves the following set of ordinary differential equations:

Droplet motion:

$$\frac{dx}{dt} = u$$

Droplet velocity change:

$$\frac{du}{dt} = \frac{3}{8}\frac{C_D}{r_s}\left(\frac{\rho_\infty}{\rho_L}\right)|u_\infty - u|(u_\infty - u) - g\left(1 - \frac{\rho_\infty}{\rho_L}\right)$$

Droplet radius change:

$$\frac{dr_s}{dt} = -\frac{\dot{m}}{4\pi\rho_L r_s^2}$$

Droplet temperature change:

$$\frac{dT_s}{dt} = \frac{1}{m_L C_{pL}}(Q_L)$$

The following steps are followed in the solution of the above equations:

1. The molar and mass fuel vapor fractions at the droplet surface are calculated

$$x_{Fs} = \frac{P_{Fs}}{P}, Y_{Fs} = \frac{x_{Fs} W_F}{\sum_i x_i W_i}$$

Here, the fuel vapor saturated pressure is evaluated using the appropriate Antoine equation of the form,

$$log_{10} P_{Fs} = A - \frac{B}{C + T}$$

2. Average physical properties in the gas film are evaluated at the reference temperature. The reference temperature is calculated using the 1/3rd rule by Yuan and Chen [13] as,

$$\bar{T} = T_s + \frac{1}{3}(T_\infty - T_s)$$

3. The droplet Reynolds number is calculated using,

$$Re = 2\rho_\infty |u - u_\infty| \frac{r_s}{\mu_g}$$

The Nusselt and Sherwood numbers for a non-vaporizing droplet are calculated using,

$$Nu_0 = 2 + 0.552 Re^{1/2} Pr^{1/3}; \quad Sh_0 = 2 + 0.552 Re^{1/2} Sc^{1/3}$$

4. The Spalding mass transfer number is calculated as,

$$B_M = \frac{Y_{Fs} - Y_{F,\infty}}{1 - Y_{Fs}}$$

The diffusional film correction factor is calculated as,

$$F_M = (1 + B_M)^{0.7} \frac{ln(1 + B_M)}{B_M}$$

The modified Sherwood number for an evaporating droplet is calculated using,

$$Sh^* = 2 + \frac{(Sh_0 - 2)}{F_M}$$

The instantaneous droplet vaporization rate is calculated using,

$$\dot{m} = 2\pi \bar{\rho}_g \bar{D}_g r_s Sh^* ln(1 + B_M)$$

5. The correction factor for the thermal film thickness is calculated iteratively using,

$$B_T = (1 + B_M)^{\varphi} - 1; \quad \varphi = \left(\frac{\bar{C}_{pF}}{\bar{C}_{pg}}\right)\left(\frac{Sh^*}{Nu^*}\right)\left(\frac{Pr}{Sc}\right); \quad Nu^* = 2 + \frac{(Nu_0 - 2)}{F_T}; \quad F_T = (1 + B_T)^{0.7} \frac{ln(1 + B_T)}{B_T}$$

6. The heat transfer into the liquid phase is calculated using,

$$Q_L = \dot{m}\left(\frac{\bar{C}_{pF}(T_\infty - T_s)}{B_T} - L(T_s)\right)$$

7. The drag coefficient is based on the correlation,

$$C_D = 27 Re_d^{0.84}$$

The equation set was solved in MATLAB using an ode solver (ode45). The equations were integrated for a period of time consistent with that observed in the experiments. The initial conditions for the droplet and ambient gas were chosen consistent with the experiment. Due to space constraints, the nomenclature used in the model is not presented here but can be found in the original work by Abramzon and Sirignano [12].

Results and Discussion

Droplet evaporation analysis

Figure 4 shows an image acquired by the camera for the case of droplet generation using pure *n*-heptane. Two successive droplets can be seen in the image. The glass nozzle whose tip is observed in the image has a diameter of 35 µ.m. Figure 5 shows a series of results from simulations and experiments for the evaporation of droplets consisting of 100% *iso*-octane and 100% n-heptane. Results are presented for an ambient temperature of 40°C. Considering the experimental results, the droplet diameter for both fuels decreases in a linear fashion with time. The plot of non-dimensionalized area ($d^2/d0^2$) shows that *n*-heptane evaporates at a faster rate than *iso*-octane. This is consistent with the lower boiling point of *n*-heptane over that of *iso*-octane as well as the higher volatility of *n*-heptane as compared to *iso*-octane. The higher volatility of *n*-heptane is reflected by the octane number of 0 assigned to it on the octane rating scale. *Iso*-octane has an octane number of 100 given its lower volatility. The droplet velocity shows a rapid decline for both fuels in the initial stages (0-10 µ.s) followed by a very slow rate of decrease. The drag force is proportional to the square of the droplet velocity. This force has a large value initially as the droplet is ejected from the nozzle with the initial velocity. This causes the rapid decrease in initial velocity

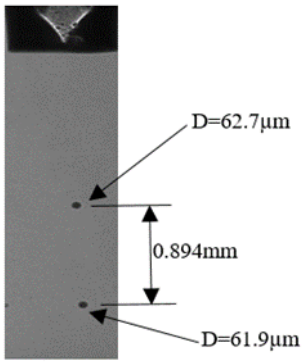

Figure 4: Camera image showing a trail of n-heptane droplets leaving the nozzle.

of the droplet. The trends in droplet velocity are consistent with the droplet displacement, which is seen to be large initially followed by a linear behaviour as the droplet velocity approaches a constant value. With regard to the simulation results, the evaporation behaviour of *n*-heptane is well captured but the simulation appears to over-estimate the evaporation rate for *iso*-octane. However, the velocity variation and displacement of the droplet predicted by the simulations are in close agreement with the experimental results. More work is required particularly on the estimation of the liquid film thermodynamic properties and their variation with temperature for *iso*-octane to improve the model accuracy.

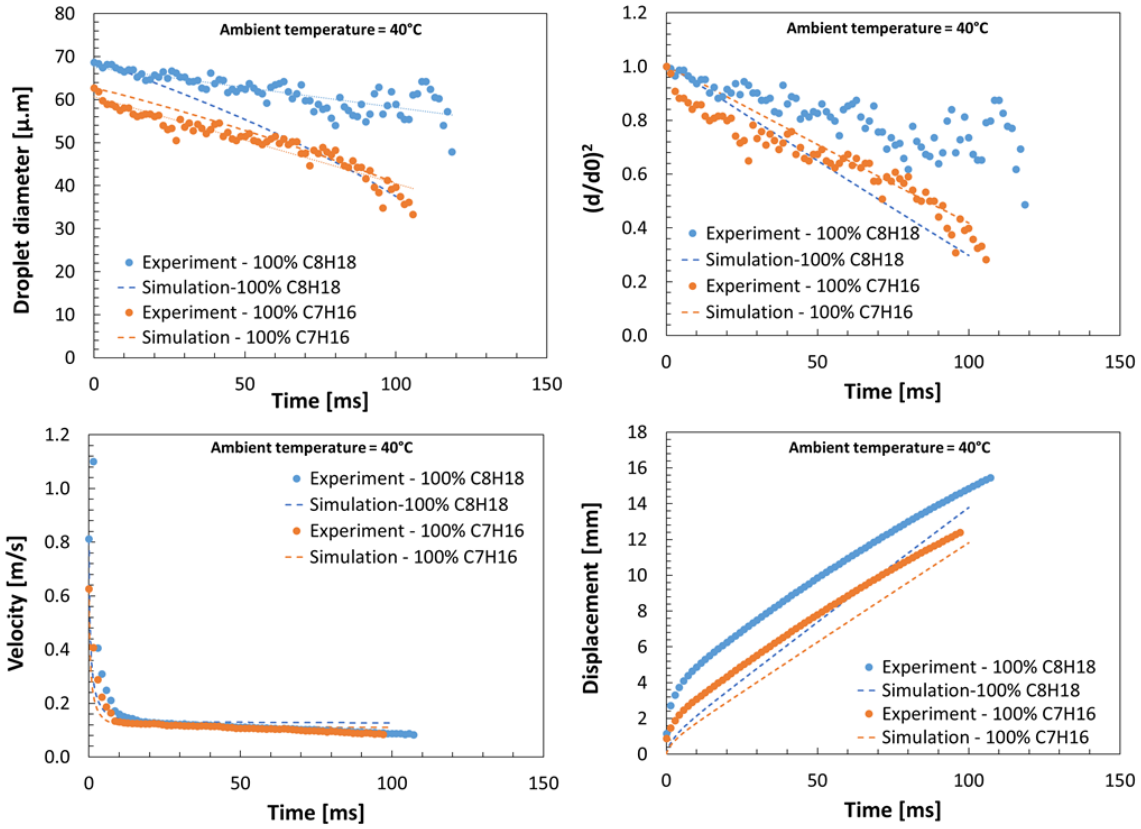

Figure 5: Results for pure iso-octane and pure n-heptane droplet evaporation at 40 deg C.

Effect of ambient temperature

Figure 6 shows the non-dimensional area change for a variety of fuel blends at two different ambient temperatures, that of 40°C and 50°C. Considering the results for 100% C_8H_{18}, as expected the evaporation rate is observed to increase with increase in ambient temperature. This trend is also captured by the simulation results. As observed previously, the simulation results over-predict the evaporation rate. Considering the results for 100% C_7H_{16}, the effect of ambient temperature change on the evaporation rate is observed to be negligible. This trend is observed both in the simulation and experimental results. It is not evident as to why the effect of increased ambient temperature is not reflected in the evaporation rate of droplets containing 100% C_7H_{16}. However, considering the remaining plots in Figure 6, the effects of increase in ambient temperature are more evident. For all the remaining fuel blends, the increase in ambient temperature is reflected by an increase in the rate of evaporation regardless of the fuel blend. It is to be noted that the simulations were only carried out for the cases of 100% C_8H_{18} and 100% C_7H_{16}. The computational model is currently being improved to incorporate multi-component fuels and once completed will be used to obtain results that can be compared with experimental data for fuel blends presented in this work.

Effect of fuel blends

Figure 7 shows the non-dimensional area change as a function of time for the various fuel blends tested in this work at an ambient temperature of 40°C. For all cases, as expected the ratio of ($d^2/d0^2$) decreases with time. The figure also show linear fits to the data sets. The evaporation rate for 100% C_8H_{18} is observed to be the slowest. As C_7H_{16} is added to the mixture, the evaporation rate begins to increase as observed by the increasing slopes for the cases having 20% and 40% C_7H_{16}. This behaviour reaches its peak with 60% C_7H_{16} in the fuel blend. However, with further increase in C_7H_{16}, the trend is seen to reverse with the evaporation rate decreasing for the cases

containing 80% C_7H_{16} and 100% C_7H_{16}. This result is interesting since it suggests that there is a non-linear change in evaporation rate with varying fuel blending ratios of PRF's.

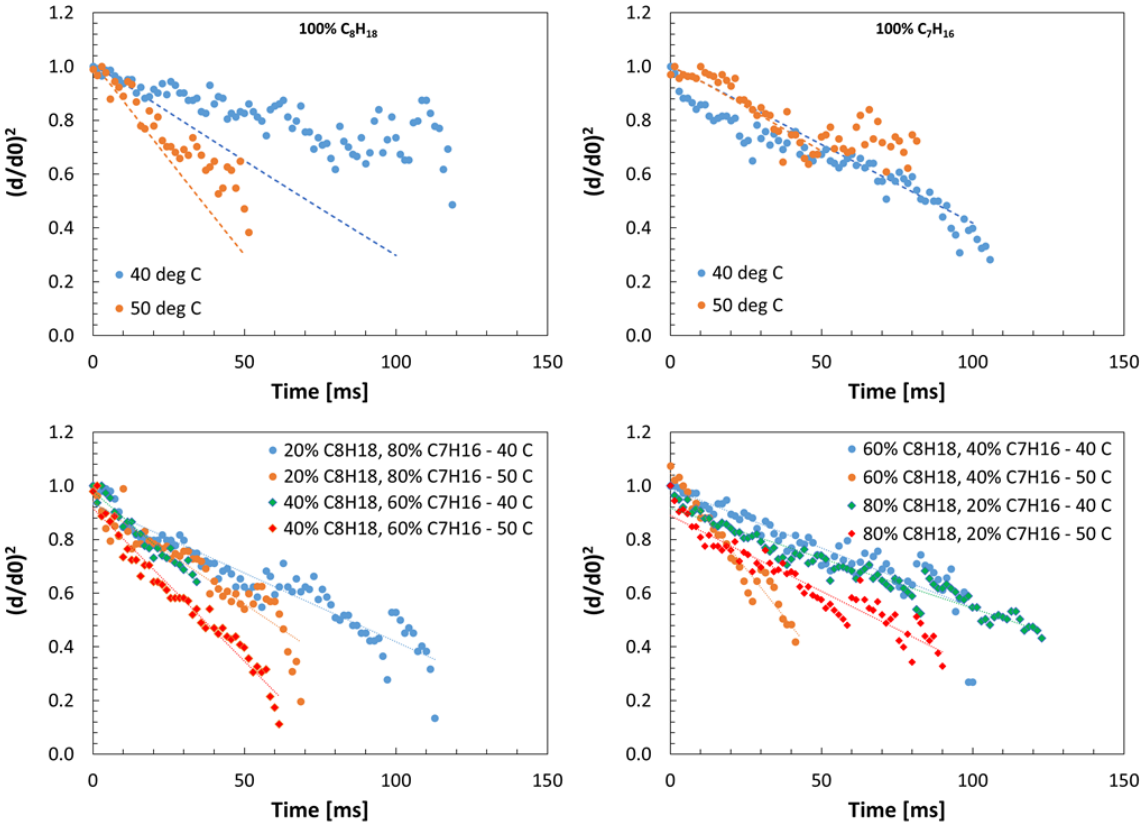

Figure 6: Non-dimensional area change for various fuel blends at two different ambient temperatures.

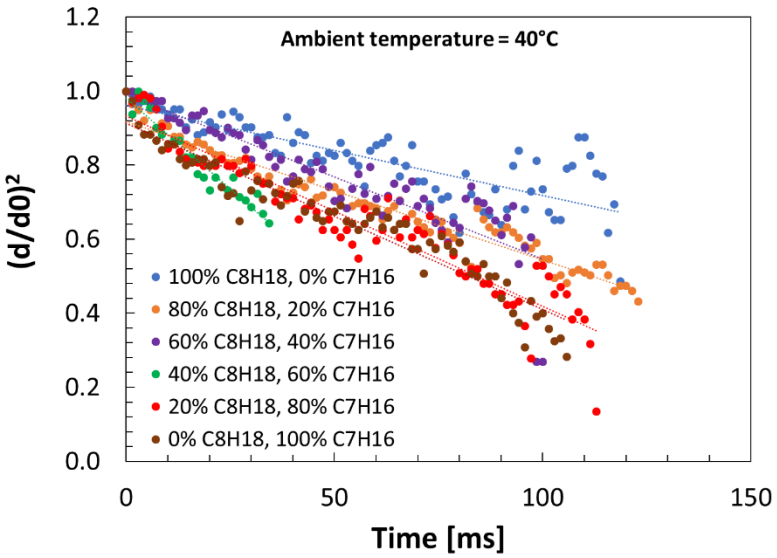

Figure 7: Non-dimensional area change showing the effect of fuel blends at 40°C

Summary and Conclusions

An experimental and computational study of the evaporation of single droplet trains of blends of primary reference fuels was carried out at elevated temperature conditions. The evaporation of droplets of *iso*-octane and *n*-heptane mixtures, generated by a piezoelectric actuator was studied at atmospheric conditions and at two different ambient temperatures of 40°C and 50°C. The higher volatility of n-heptane over that of *iso*-octane was reflected in the faster evaporation rate as captured by both simulation and experimental results. However, the

simulation results over-predict the evaporation rate of n-hepane. Droplet velocity change and displacement trends were consistent between simulations and experiments. The increase in ambient temperature is seen to increase the evaporation rate of pure iso-octane droplets. However, this is less apparent for pure n-heptane droplets. For all the intermediate fuel blends, the increase in evaporation rate with increase in ambient temperature is captured by the experiments. For a constant ambient temperature, addition of more volatile *n*-heptane to *iso*-octane is seen to initially increase the evaporation rate. However, this behavior peaks for a 40% *iso*-octane 60% *n*-heptane volumetric blend. With further increase in *n*-heptane concentration, the evaporation rate is observed to decrease. Further investigation is required to understand this behavior. Future work will focus on development of the model to account for evaporation of multi-component fuels. The experiments will be extended to higher pressures and higher temperatures that are more representative of cylinder conditions in advanced internal combustion engines.

Acknowledgements

This research was conducted as part of the Co-Optimization of Fuels & Engines (Co-Optima) project sponsored by the U.S. Department of Energy (DOE) Office of Energy Efficiency and Renewable Energy (EERE), Bioenergy Technologies and Vehicle Technologies Offices.

References

[1] Dec, J., Yang, Y., Dernotte, J., and Ji, C., "Effects of Gasoline Reactivity and Ethanol Content on Boosted, Premixed and Partially Stratified Low-Temperature Gasoline Combustion (LTGC)," SAE Int. J. Engines, vol. 8, no. 3, pp. 935–955, 2015.

[2] Reitz, R. D. and Duraisamy, G., "Review of high efficiency and clean reactivity controlled compression ignition (RCCI) combustion in internal combustion engines," Prog. Energy Combust. Sci., vol. 46, pp. 12–71, 2015.

[3] Dempsey, A. B., Curran, S. J., and Wagner, R. M., "A perspective on the range of gasoline compression ignition combustion strategies for high engine efficiency and low NOx and soot emissions: Effects of in-cylinder fuel stratification," Int. J. Eng. Res., vol. 17, pp. 897–917, October 2016.

[4] McCormick, R. L., Fioroni, G., Fouts, L., Christensen, E., Yanowitz, J., Polikarpov, E., & George, A. (2017). Selection criteria and screening of potential biomass-derived streams as fuel blendstocks for advanced spark-ignition engines. *SAE International Journal of Fuels and Lubricants*, *10*(2017-01-0868), 442-460.

[5] Bassett, M., Hall, J., Hibberd, B., Borman, S., Reader, S., Gray, K., and Richards, B., "Heavily Downsized Gasoline Demonstrator," SAE Int. J. Engines, vol. 9, no. 2, pp. 729–738, 2016.

[6] Sazhin, S. S. (2006). Advanced models of fuel droplet heating and evaporation. *Progress in energy and combustion science*, *32*(2), 162-214.

[7] Birouk, M., & Gökalp, I. (2006). Current status of droplet evaporation in turbulent flows. *Progress in energy and combustion science*, *32*(4), 408-423.

[8] Peng, F., & Aggarwal, S. K. (1994, June). A review of droplet dynamics and vaporization modeling for engineering calculations. In *ASME 1994 International Gas Turbine and Aeroengine Congress and Exposition* (pp. V003T06A003-V003T06A003). American Society of Mechanical Engineers.

[9] Sirignano, W. A. (1983). Fuel droplet vaporization and spray combustion theory. *Progress in Energy and Combustion Science*, *9*(4), 291-322.

[10] AlAbbad, M., Javed, T., Khaled, F., Badra, J., & Farooq, A. (2017). Ignition delay time measurements of primary reference fuel blends. *Combustion and Flame*, *178*, 205-216.

[11] Schneider, C. A.; Rasband, W. S. & Eliceiri, K. W. (2012), "NIH Image to ImageJ: 25 years of image analysis", Nature methods 9(7): 671-675.

[12] Abramzon, B., & Sirignano, W. A. (1989). Droplet vaporization model for spray combustion calculations. International journal of heat and mass transfer, 32(9), 1605-1618.

[13] M. C. Yuen and L. W. Chen. On drag of evaporating liquid droplets. Combust. Sci. Technol. 14, 147-154 (1976).

[14] Renksizbulut, M., & Haywood, R. J. (1988). Transient droplet evaporation with variable properties and internal circulation at intermediate Reynolds numbers. International journal of multiphase flow, 14(2), 189-202.